Hafnium Oxide and Zirconium Oxide Atomic Layer Deposition: Initial Precursor and Potential Side-Reaction Product Pathways with H/Si(100)-2×1

Ryan D. Fenno, Mathew D. Halls, and Krishnan Raghavachari*

Department of Chemistry, Indiana University, Bloomington, Indiana 47405

Received: March 25, 2004; In Final Form: January 17, 2005

Hybrid density functional calculations have been carried out using cluster models of the H/Si(100)-2×1 surface to investigate the mechanistic details of the initial surface reactions occurring in the atomic layer deposition of hafnium and zirconium oxides (HfO_2 and ZrO_2). Reaction pathways involving the metal precursors $ZrCl_4$, $Zr(CH_3)_4$, $HfCl_4$, and $Hf(CH_3)_4$ have been examined. Pathways leading to the formation of a Zr−Si or Hf−Si linkage show a significant sensitivity to the identity of the leaving group, with chloride loss reactions being both kinetically and thermodynamically less favorable than reactions leading to the loss of a methyl group. The energetics of the $Zr(CH_3)_4$ and $Hf(CH_3)_4$ reactions are similar with an overall exothermicity of 0.3−0.4 eV and a classical barrier height of 1.1−1.2 eV. For the reaction between H_2O and the H/Si(100)-2×1 surface, the activation energy and overall reaction enthalpy are 1.6 and −0.8 eV, respectively. Due to contamination, trace amounts of H_2O may be encountered by metal precursors, leading to the formation of minor species that can lead to unanticipated side-reaction pathways. Such gas-phase reactions between the halogenated and alkylated metal precursors and H_2O are exothermic with small or no reaction barriers, allowing for the possibility of metal precursor hydroxylation before the H/Si surface is encountered. Of the contaminant surface reaction pathways, the most kinetically favorable corresponds to the surface −OH deposition. Interestingly, for the hydroxylated metal precursors, a unique reaction pathway resulting in the direct formation of Si−O−Zr and Si−O−Hf linkages has been identified and found to be the most thermodynamically stable pathway available, being exothermic by ∼1.0 eV.

I. Introduction

Continued miniaturization in the semiconductor industry in accordance with "Moore's law" will render SiO_2 unusable as a gate oxide layer within a decade.[1] Therefore, the search for alternative materials to replace SiO_2 has been a critical area of research in recent years.[2] The most promising high-κ replacement materials under investigation are the binary metal oxides. Two such materials that have received widespread attention are zirconium oxide (ZrO_2) and hafnium oxide (HfO_2). These materials have a number of attractive characteristics such as forming thermodynamically stable interfaces with silicon[3,4] and having much larger dielectric constants ($\kappa \approx 25$) compared to SiO_2 ($\kappa = 3.9$).[5] Materials with a higher dielectric constant will permit the use of thicker gate oxide layers with the desired capacitances, while minimizing tunneling current in semiconductor devices.[6]

As active layer thicknesses approach the nanometer regime, an additional concern is the development of deposition techniques which allow for the conformal growth of high-quality uniform thin solid films. The predominant experimental growth technique meeting this requirement is atomic layer deposition (ALD), which is based on performing successive, self-terminating half-reactions on a substrate surface,[7] giving rise to controlled growth of up to one monolayer per exposure. In the case of the ALD of metal oxides, the necessary half-reactions are comprised of exposing the surface to a metal precursor, followed by an oxygen precursor (typically water), depositing one atomic layer per pulse.[4,8,9] The reaction mechanism and energetics for ALD growth of ZrO_2 and HfO_2 have been the topic of recent reports. For example, Ritala and co-workers have carried out experiments demonstrating the ALD growth of ZrO_2 and HfO_2 films, obtaining uniform and self-controlled growth that is characteristic of the reactive and sequential nature of ALD.[10,11] Musgrave and co-workers[12,13] carried out complementary theoretical studies using density functional theory, representing the growing film with metal oxide clusters, to identify the dominant growth mechanisms and energetics for the ALD of ZrO_2 and HfO_2 using the respective metal tetrachlorides and water as precursors. However, the atomistic details of the initial surface reaction pathways for the ZrO_2 and HfO_2 ALD precursors on many technologically relevant substrates are still largely unknown.

Work by Chabal and co-workers,[14] investigating the nucleation of ALD growth of Al_2O_3 on hydrogen-passivated silicon (H/Si) surfaces, suggests that, for some systems, the initiation of deposition requires exposure, first to the metal precursor rather than to H_2O. Also, infrared measurements made after the initial exposure of the H/Si surface to the Al precursor $Al(CH_3)_3$ (TMA) indicated the possible formation of oxygen-containing surface linkages,[15] which were attributed to surface reactions of a gas-phase side-reaction product. In particular, trace amounts of water in the reaction chamber or precursor stream may react with the metal precursor before impinging on the H/Si substrate, leading to new surface reaction pathways. Therefore, in addition to surface reaction pathways between H/Si and H_2O, and the basic metal precursors, other surface chemistries involving the hydroxylated metal precursors might also be investigated as they

* To whom correspondence should be addressed. E-mail: kraghava@indiana.edu.

10.1021/jp048663g CCC: $30.25
Published on Web 02/23/2005

might play a minor role in interface formation in the early stages of ALD deposition.

In the work presented here, calculations based on hybrid density functional theory are carried out on silicon cluster models to investigate the chemical mechanisms and details of the initial reaction pathways for ALD growth of ZrO_2 and HfO_2 on the hydrogen-passivated Si(100)-2×1 surface. Pathway activation energies and enthalpies are calculated for the widely used halogenated metal precursors zirconium tetrachloride[10,16−18] ($ZrCl_4$) and hafnium tetrachloride[11,19−21] ($HfCl_4$) and the oxygen precursor H_2O. For comparison with the chlorinated precursor results, initial surface reactions involving the tetraalkylated metal precursors tetramethylzirconium ($Zr(CH_3)_4$) and tetramethylhafnium ($Hf(CH_3)_4$) are also studied. These tetraalkylated compounds were chosen as a means of investigating the energetics of general tetraalkylated precursor deposition, while minimizing steric effects that are present in larger, more stable titanium group tetraalkyls.[22−24] Comparison of the relative reaction energetics provides critical insight into the functional group and metal center dependencies, as well as the effect of precursor hydroxylation, with possible implications for ZrO_2 and HfO_2 ALD nucleation.

II. Computational Methods

The reaction site on the hydrogen-terminated Si(100)-2×1 surface was represented by a constrained Si_9H_{14} cluster, as employed successfully in many previous studies.[25−29] This cluster corresponds to approximately one unit cell of the 2×1 reconstructed H/Si(100) surface and, therefore, restricts the reactions under consideration to a single dimer of the reconstructed surface. Given the respective sizes of the gas-phase reactants, interactions with neighboring dimers are not expected to affect the overall chemistry. To avoid artifacts due to excess spin or charge, the cluster is terminated with hydrogen atoms, which satisfy the valency of the Si−Si bonds that were cleaved during excision from the extended surface. To mimic the mechanical constraints of the extended surface and inhibit unphysical structural relaxation, boundary conditions are applied.[26,27] The three silicon atoms corresponding to the third and fourth layers and the eight hydrogen atoms representing third-, fourth-, and fifth-layer silicon atoms were fixed to ideal tetrahedral bonding positions of bulk silicon with Si−H distances of 1.48 Å and Si−Si distances of 2.35 Å. The positions of all other atoms were allowed to vary throughout the structural optimizations. The resulting minimum energy geometries of the reactants, transition structures, products, and complexes of the various gas-phase and surface reactions were calculated and subsequently verified by harmonic frequency calculations.

The calculations described here were carried out using the Gaussian 03 electronic structure package.[30] The B3-LYP hybrid density functional was used, which corresponds to Becke's three-parameter exchange functional (B3) along with the Lee−Yang−Parr gradient-corrected correlation functional (LYP).[31,32] The basis set employed in this work was of a multilevel quality, denoted dzp, with the metal atoms (Hf and Zr) being represented by the LANL2DZ pseudopotential basis set[33−35] with additional s, p, d, and f diffuse functions (derived from energy minimizations on the metal chlorides $ZrCl_4$ and $HfCl_4$)[36] and all other atoms being represented with the 6-31G* Pople basis set.[37]

Model chemistries of this type have been employed extensively in similar computational studies[12,13,15,38,39] due to the computational efficiency and good quantitative performance. The B3-LYP hybrid functional is often the method of choice to examine the mechanism and energetics of chemical processes in materials chemistry. In a previous study on the ALD reactions for Al_2O_3 growth using similar cluster models, we calibrated the B3-LYP results by comparison with accurate coupled-cluster energy calculations including contributions from single, double, and perturbative triple excitations [CCSD(T)] with a medium-sized basis set (similar to dzp).[40] It was found that the B3-LYP results were quite accurate, the higher levels of electron correlation favoring the transition state and product by only about 0.1 eV. If a similar behavior persists for the current systems, the barriers and overall enthalpies presented in this work may be slightly more favorable than indicated by the B3-LYP/dzp results. Furthermore, all enthalpies reported here include zero-point energy (ZPE) corrections.

III. Results and Discussion

ALD growth of ZrO_2 and HfO_2 involves the exposure of the substrate to alternating gas-phase metal and oxygen precursors with film growth proceeding through self-terminating surface reactions. For instance, in the case of ZrO_2 deposition using $ZrCl_4$ and H_2O as ALD precursors, the reaction sequence would involve reaction of $ZrCl_4$ with substrate surface O−H groups, liberating HCl and depositing $-ZrCl_3$ on the surface. Following a purge period, subsequent exposure to H_2O would form a Zr−OH linkage, again releasing HCl. This mechanism was investigated by Widjaja, Han, and Musgrave using quantum chemical methods.[12] In the current paper we describe the initial surface reactions between the H/Si(100) surface and the basic ALD precursors $ZrCl_4$, $Zr(CH_3)_4$, $HfCl_4$, and $Hf(CH_3)_4$, and H_2O, as well as potential alternative surface reactions stemming from minor gas-phase side-reaction products.

A. Reactions between the Basic ALD Precursors and H/Si-(100)-2×1. Depending on the system and reactor conditions used, the initial exposure of the H/Si substrate can be to either a metal precursor or an oxygen precursor to nucleate the ALD process. Initial reaction with a metal precursor, MR_4 (M = Zr or Hf and R = Cl or CH_3), and the H/Si(100)-2×1 surface results in the formation of a M−Si linkage and a H−R leaving group:

$$Si{-}H^* + MR_4 \rightarrow Si{-}MR_3^* + HR \qquad (MR1)$$

where an asterisk denotes a surface species. As oxide thicknesses continue to decrease, an understanding of the atomistic details and thermochemistry of the initial surface reactions between ALD precursors and the H/Si substrate will become vital in the controlled creation of abrupt interfaces between bulk silicon and high-quality metal oxide films. The reaction coordinates for the deposition of the precursors $ZrCl_4$, $Zr(CH_3)_4$, $HfCl_4$, and $Hf(CH_3)_4$ are presented in Figures 1−4, respectively, and are denoted by open squares.

As the metal precursors approach the reaction site on the surface, a reactant-like complex can form between the metal center and the hydrogen-passivated surface. As expected for a nonpolar surface, such complexes are only very weakly bound. For the zirconium reactions, these complexes are only 0.03 and 0.01 eV lower in energy than the separated reactants for R = Cl and CH_3, respectively. The corresponding energies for the analogous complexes formed with the hafnium precursors are 0.07 and 0.01 eV, respectively. Hence, the chlorinated species form slightly more strongly bound surface complexes than the methylated species. It must be noted that although these reactant complexes are true minima on the B3LYP/dzp potential energy surface, the weak nature of the binding implies that adsorption of the precursors considered here with the H/Si surface is not

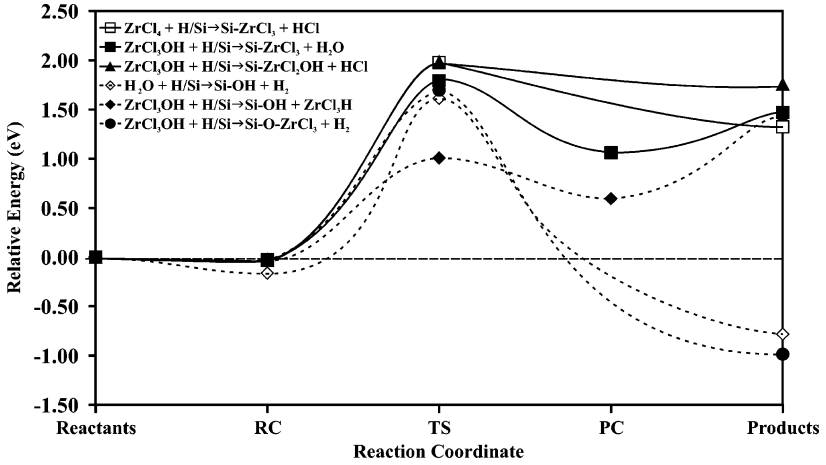

Figure 1. Reaction energy profiles for the initial surface reaction pathways of $ZrCl_4$, H_2O, and $ZrCl_3OH$ with the H/Si(100)-2×1 surface calculated at the B3-LYP/dzp level of theory. Filled symbols represent $ZrCl_3OH$ reactions, while open symbols represent $ZrCl_4$ and H_2O reactions.

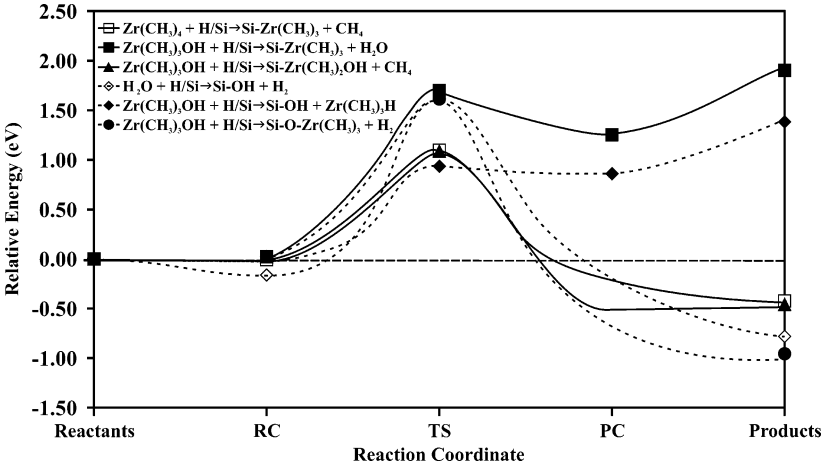

Figure 2. Reaction energy profiles for the initial surface reaction pathways of $Zr(CH_3)_4$, H_2O, and $Zr(CH3)_3OH$ with the H/Si(100)-2×1 surface calculated at the B3-LYP/dzp level of theory. Filled symbols represent $Zr(CH_3)_3OH$ reactions, while open symbols represent $Zr(CH_3)_4$ and H_2O reactions.

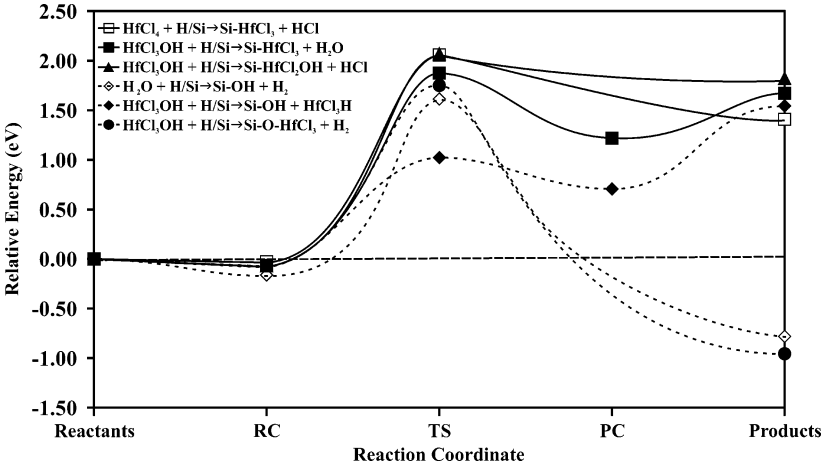

Figure 3. Reaction energy profiles for the initial surface reaction pathways of $HfCl_4$, H_2O, and $HfCl_3OH$ with the H/Si(100)-2×1 surface calculated at the B3-LYP/dzp level of theory. Filled symbols represent $HfCl_3OH$ reactions, while open symbols represent $HfCl_4$ and H_2O reactions.

expected to occur (unlike bare and hydroxylated silicon substrates).[12]

Following its initial approach, the metal precursor can react with the dimer Si−H, leading to deposition of $-MR_3$ and the release of HR. Representative bond lengths and reaction enthalpies are presented in Tables 1 and 2 for Zr and Hf reactions, respectively. For the chlorinated species, the classical barrier heights for Si−M linkage formation are 1.98 and 2.06 eV for Zr and Hf. The transition states for this pathway have Si−Zr and Si−Hf bond lengths of 2.85 and 2.81 Å, which are 0.16 and 0.14 Å longer than those in the surface products. Overall these reactions are calculated to be significantly endothermic, having reaction enthalpies of 1.32 and 1.41 eV for Zr and Hf. These results are in qualitative agreement with previous work by Musgrave and co-workers,[12] who also found that the formation of a Si−Zr linkage requires passage through

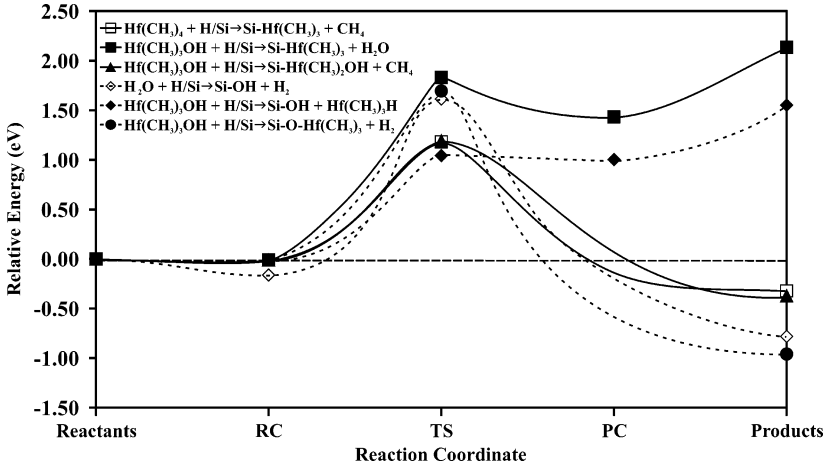

Figure 4. Reaction energy profiles for the initial surface reaction pathways of $Hf(CH_3)_4$, H_2O, and $Hf(CH_3)_3OH$ with the H/Si(100)-2×1 surface calculated at the B3-LYP/dzp level of theory. Filled symbols represent $Hf(CH3)_3OH$ reactions, while open symbols represent $Hf(CH_3)_4$ and H_2O reactions.

TABLE 1: Relative Enthalpies and Representative Bond Lengths for the Gas-Phase Reactions between the Metal Precursors MR_4 and H_2O Leading to the Formation of MR_3OH Calculated at the B3-LYP/dzp Level of Theory

	representative bond lengths (Å)							
	reactants	transition structures			products	relative enthalpies[a] (eV)		
M, R	M−R	M−R	H−O	M−O	M−O	RC	TS	products
Zr, Cl	2.33	2.85	1.35	2.06	1.89	−0.80	0.04	−0.15
Zr, CH_3	2.23	2.46	1.15	2.23	1.93	−0.47	−0.19	−2.34
Hf, Cl	2.31	2.81	1.35	2.03	1.87	−0.83	−0.04	−0.29
Hf, CH_3	2.21	2.43	1.14	2.20	1.90	−0.51	−0.21	−2.48

[a] ZP-corrected relative enthalpies with respect to the separated reactants.

TABLE 2: Representative Bond Lengths (Å) for the Critical Point Structures for the Reactions of the Zr Precursors with the H/Si(100) Surface Calculated at the B3-LYP/dzp Level of Theory[a]

reaction products	transition structures				product complex				products	
(Si−D + L)	L−D	Si−H	Si−D	L−H	L−D	Si−H	Si−D	L−H	Si−D	L−H
Si−$ZrCl_3$ + HCl	2.81	2.07	2.85	1.43					2.69	1.29
Si−$ZrCl_3$ + H_2O	2.12	1.81	3.05	1.28	2.37	3.33	2.74	0.98	2.69	0.97
Si−$ZrCl_2OH$ + HCl	2.87	2.08	2.85	1.43					2.71	1.29
Si−OH + $ZrCl_3H$	2.08	1.65	2.00	2.05	2.29	2.82	1.76	1.84	1.69	1.82
Si−O−$ZrCl_3$ + H_2	1.44	1.76	2.27	0.87					1.71	0.74
Si−$Zr(CH_3)_3$ + CH_4	2.37	1.77	3.07	1.58					2.77	1.09
Si−$Zr(CH_3)_3$ + H_2O	2.16	1.85	3.23	1.23	2.39	3.03	2.85	0.98	2.77	0.97
Si−$Zr(CH_3)_2OH$ + CH_4	2.38	1.77	3.09	1.58					2.77	1.09
Si−OH + $Zr(CH_3)_3H$	2.14	1.60	1.96	2.11	2.32	2.42	1.75	1.92	1.69	1.87
Si−O−$Zr(CH_3)_3$ + H_2	1.13	1.79	1.86	1.17					1.67	0.74

[a] The letters "L" and "D" denote the leaving and surface-deposited groups that together make up the metal precursor of the particular reaction.

a high-energy transition structure, with the overall process being quite endothermic. Using a slightly different model where one of the surface hydrogens is replaced by a hydroxyl group, they computed an activation energy of 1.34 eV and an overall enthalpy of 0.95 eV. The influence of the hydroxyl group is evidently substantial.

As shown in Figures 2 and 4, the reaction profiles involving methylated precursors are similar for Zr and Hf. An important observation is that, in contrast to the chlorinated precursor reactions, the methylated precursor reactions are thermodynamically favorable, being exothermic by 0.43 and 0.32 eV, for Zr and Hf, respectively. This clearly is a consequence of the relatively weaker nature of the $M-CH_3$ bond being broken (relative to that of M−Cl).[41] The transition structures have M−C and Si−M bond lengths of 2.37 and 2.35 Å and 3.07 and 3.06 Å for Zr and Hf metal centers, respectively. The activation energies for the $-M(CH_3)_3$ deposition reactions are 1.10 (Zr) and 1.18 (Hf) eV, significantly lower than the energy barriers for the chlorinated precursors. Clearly, the alkylated metal precursor surface reaction pathways are both kinetically and thermodynamically more favorable than the halogenated metal precursor pathways.

The initial surface reaction pathway with the oxygen precursor entails H_2O reacting with the H/Si(100) surface, leaving behind a surface O−H group and releasing H_2:

$$Si-H^* + H_2O \rightarrow Si-OH^* + H_2$$

The reaction energy profile for H/Si hydroxylation by H_2O is shown in Figure 1 (denoted by ◇). At the B3-LYP/dzp level of theory, the H_2O adsorption energy on the H/Si(100)-2×1 surface is 0.16 eV. Previously, Akagi and Tsukada[42] carried out density functional calculations (GGA-II) using a slab model and a plane wave pseudopotential basis and determined the adsorption energy for H_2O on the surface to be 0.16 eV. The results presented here are in good agreement. Additionally, earlier work in our own group using a Si_9H_{14} cluster along with B3-LYP

TABLE 3: Representative Bond Lengths (Å) for the Critical Point Structures for the Reactions of the Hf Precursors with the H/Si(100) Surface Calculated at the B3-LYP/dzp Level of Theory[a]

reaction products	transition structures				product complex				products	
(Si−D + L)	L−D	Si−H	Si−D	L−H	L−D	Si−H	Si−D	L−H	Si−D	L−H
Si−$HfCl_3$ + HCl	2.79	2.09	2.81	1.42					2.67	1.29
Si−$HfCl_3$ + H_2O	2.09	1.83	3.01	1.26	2.33	3.37	2.72	0.98	2.67	0.97
Si−$HfCl_2OH$ + HCl	2.85	2.09	2.83	1.42					2.70	1.29
Si−OH + $HfCl_3H$	2.04	1.66	2.01	2.02	2.25	2.81	1.77	1.83	1.69	1.81
Si−O−$HfCl_3$ + H_2	1.42	1.75	2.23	0.88					1.70	0.74
Si−$Hf(CH_3)_3$ + CH_4	2.35	1.79	3.06	1.55					2.75	1.09
Si−$Hf(CH_3)_3$ + H_2O	2.13	1.89	3.23	1.20	2.36	3.03	2.84	0.98	2.75	0.97
Si−$Hf(CH_3)_2OH$ + CH_4	2.38	1.80	3.07	1.55					2.75	1.09
Si−OH + $Hf(CH_3)_3H$	2.10	1.60	1.96	2.10	2.29	2.48	1.76	1.91	1.69	1.86
Si−O−$Hf(CH_3)_3$ + H_2	1.13	1.78	1.88	1.17					1.68	0.74

[a] The letters "L" and "D" denote the leaving and surface-deposited groups that together make up the metal precursor of the particular reaction.

and a larger 6-311G(2df,2p) basis set also yielded an adsorption energy of 0.15 eV.[39]

The overall surface hydroxylation reaction is found to be exothermic, with the reaction products being 0.78 eV lower in energy than the separated reactants. The classical barrier height for hydroxylation of the H/Si(100)-2×1 surface is quite large, 1.61 eV. As with the surface binding energy, these energies are in excellent agreement with the exothermicity and activation energy, obtained using a larger basis set, of 0.75 and 1.60 eV.[39] Kang and Musgrave,[43] using hybrid density functional theory and the 6-311+G(d,p) basis set, examined the reaction of H_2O at the neighboring hydrogen of a partially hydroxylated H/Si-(100) surface using a cluster model similar to that employed in the present work. The activation energy and exothermicity for the hydroxylation of the second dimer Si was predicted to be 1.44 and 0.23 eV, respectively. The lower exothermicity relative to our value is probably indicative of the decreased stability of a dimer containing two hydroxyl groups.

A comparison of the reaction enthalpies and barrier heights for the initial surface reaction pathways of the different precursors with the H/Si(100)-2×1 surface provides critical insight into ALD nucleation at modest temperatures and reactor conditions. At the B3-LYP/dzp level of theory, the H_2O initial surface reaction, leading to deposition of −OH, has an energy barrier at least 0.37 eV lower than those of the MCl_4 surface pathways, whereas the $M(CH_3)_4$ reaction paths have activation energies at least 0.43 eV lower than for that of the surface hydroxylation pathway. For alkylated precursors, it may be judicious to nucleate the ALD process by initial treatment of the H/Si substrate with the metal precursor, as found in the case of Al_2O_3 using trimethylaluminum,[14] whereas ALD using halogenated precursors may require surface hydroxylation as the initial step.

B. Gas-Phase Side Reaction between ALD Precursors and H_2O. Prior to encountering the H/Si(100)-2×1 substrate, the Hf and Zr metal precursors may undergo a side reaction with contaminant H_2O in the deposition chamber, as

$$MR_4 + H_2O \rightarrow MR_3OH + RH$$

potentially resulting in additional surface reaction pathways involving the hydroxylated precursor product. Further hydroxylation of the metal precursors is assumed not to occur because of the extremely low concentration of moisture in the reaction chamber. In the case of Al_2O_3 ALD, combined infrared and theoretical investigations have implicated such hydroxylated side-reaction products in interface formation.[15] Table 3 presents the representative bond lengths of the reactants, transition structures, and products, as well as the relative enthalpies of these critical points, for these reactions where M = Zr or Hf and R = Cl or CH_3.

As shown in Table 3 the gas-phase side reactions are thermodynamically favorable, being exothermic by 0.15 and 2.34 eV for the chlorinated and methylated Zr precursors, respectively; the corresponding energies for the Hf precursors are similar, 0.29 and 2.48 eV. For a given metal center, comparison of the relative reaction enthalpies shows a large difference between the chlorinated and methylated species. The reaction with the chlorinated precursors is 2.19 eV less exothermic than for the methylated precursors and is clearly due to the strength of the M−Cl bond relative to M−CH_3. Also, the reaction enthalpies show a slight sensitivity to the identity of the metal center, with the Zr ALD precursor reactions being 0.14 eV less favorable than the Hf reactions. The activation energies in Table 3 show a similar dependence between the halogenated and alkylated species. For all the ALD precursors the hydroxylation side reaction is kinetically uninhibited, having a maximum barrier of only 0.04 eV.

Structurally, the changes in bond lengths during the course of the reaction are similar within each class of chlorinated or methylated precursors. As the chlorinated precursors progress along their respective reaction coordinates, the M−Cl bond lengthens by ca. 0.50 Å in forming the activated complex, consistent with the ultimate breaking of these bonds. Also, the H−O bond in H_2O increases by 0.38 Å from the reactants to the transition state. From the transition state, the M−O distance decreases by ca. 0.17 Å in forming the MCl_3OH product, indicating that bond formation has been completed. The changes in structure for the methylated precursors can be compared to those for the chlorinated precursors. When approaching the transition states, the transitional bonds (of the metal precursor and water) extend about half as much as for the Cl reactions, and the path from the transition structure to the separated products is characterized by a reduction in the M−O atomic distance by 0.30 Å (nearly twice the difference for the tetrachloride reactions). On going from reactants to products, the reaction passes though an initial precursor···H_2O reactant complex, which is bound by about 0.8 eV for the tetrachloride precursors and 0.5 eV for the tetramethyl precursors, before passing through a transition state that is comparable or lower in energy than the separated reactants. The overall enthalpy of reaction for the formation of MCl_3OH or $M(CH_3)_3OH$, where M = Zr, Hf, ranges from −0.15 to −2.48 eV, the larger values occurring for the methyl precursor, as expected. Therefore, at conditions employed during the ALD process, the MR_3OH species is a potential contaminant owing to the vigorous reaction between MR_4 and trace H_2O.

The energetics of the following two surface reactions, analogous to the gas-phase reactions described above for M = Zr and R = Cl, were recently reported by Widjaja et al.:[12]

$$Si-OH^* + ZrCl_4 \rightarrow Si-O-ZrCl_3^* + HCl \quad (R1)$$

$$Zr-Cl^* + H_2O \rightarrow Zr-OH^* + HCl \quad (R2)$$

where an asterisk denotes a terminal surface species. The reaction R1 is the ALD half-reaction resulting in an Si−O−Zr linkage, and R2 is the half-reaction resulting in the hydroxylation of the surface metal species. In the course of both reactions, the gas-phase reactant forms a physisorbed complex that is bound by ca. 1 eV, followed by a transition-state structure that is nearly equivalent energetically to the separated reactant species corresponding to barrier heights of −0.04 eV for R1 and 0.04 eV for R2. The overall calculated enthalpies of these two reactions are somewhat different. Reaction R1 is *exo*thermic (by 0.30 eV), whereas reaction R2 is slightly *endo*thermic (by 0.09 eV). Hence, the gas-phase side reaction between $ZrCl_4$ and water is energetically more similar to R1 than R2.

C. Reactions between the Hydroxylated Metal Precursors and H/Si(100)-2×1. In the initial ALD surface reactions, the tetrachloride or tetramethyl precursors encounter and react with the H/Si(100) surface, thus initiating thin film growth. Due to incorporation of an O−H group into the metal precursor, the hydroxylated precursors have surface reaction pathways analogous to those of both the oxide and the metal precursors, along with an additional unique chemical reaction pathway. The reaction pathways available to the hydroxylated metal precursors and H/Si(100) surface are

$$Si-H^* + MR_3OH \rightarrow Si-MR_3^* + H_2O \quad (MR2)$$

$$Si-H^* + MR_3OH \rightarrow Si-MR_2OH^* + HR \quad (MR3)$$

$$Si-H^* + MR_3OH \rightarrow Si-OH^* + MR_3H \quad (MR4)$$

$$Si-H^* + MR_3OH \rightarrow Si-O-MR_3^* + H_2 \quad (MR5)$$

where an asterisk denotes a surface species, M = Zr, Hf, and R = Cl, CH_3. MR1 was discussed earlier and corresponds to the basic ALD reaction for the specific combination of M and R. It will still be the dominant pathway since the hydroxylated precursors of the form MR_3OH are only assumed to be present in trace amounts and can only lead to isolated surface contaminants. For the hydroxylated precursors, there are two reaction pathways analogous to MR1 leading to the formation of M−Si linkages, denoted MR2 and MR3, differing in which species is released during the reaction. MR4 corresponds to a reaction analogous to the dominant H/Si reaction with H_2O, leading to hydroxylation of the surface site. MR5 has no analogue to the previously studied reactions. The reaction profiles of MR1−MR5 are shown in Figures 1−4.

Each of the surface reactions considered here involves the simultaneous abstraction of a surface hydrogen and deposition of a fragment of a metal precursor through the formation of either a Si−M or a Si−O bond. In Figures 1−4, the energy profiles for reactions leading to a Si−M bond are drawn with solid curves, and those leading to a Si−O bond are drawn with dashed curves. Tables 1 and 2 present the representative bond lengths of the optimized structures corresponding to reaction critical points during the progression of reactions MR1−MR5 for the chlorinated and methylated Zr and Hf ALD precursors.

The gas-phase side-reaction products can form reactant complexes analogous to those formed between the surface and the native ALD precursors MR_4. The bound complexes between H/Si and MR_3OH have essentially the same stabilities as the parent MR_4 complex with the exception of $HfCl_3OH$, which is more weakly bound than the native $HfCl_4$ by 0.04 eV. As noted for the reactant complexes formed during the basic ALD reactions, these energies are too small to be of significant importance in such reactions.

The surface reactions involving MR_3OH that lead to products with metal linkages are the reactions MR2 and MR3. The reaction coordinates corresponding to these reactions are denoted by ■ and ▲, respectively, in Figures 1−4. The replacement of a chlorine in MCl_4 with a hydroxyl group leads to an increased endothermicity of the metal−silicon product in MR2 by 0.15 and 0.26 eV for Zr and Hf precursors, respectively. The corresponding values for MR3 are 0.43 and 0.42 eV. The MR2 and MR3 pathways have energy barriers ca. 0.18 eV less than and 0.01 eV greater than the basic ALD reaction (MR1). Overall, reaction pathways involving the tetrachloride precursors, both basic and hydroxylated, leading to Si−Zr and Si−Hf linkages have significant activation energies (1.80−2.07 eV) and are endothermic (by 1.32 to 1.82 eV). This is understandable since the M−Cl or M−OH bonds that are broken in such reactions are both very strong.[44]

The effect of hydroxylation on the methylated reaction enthalpies is markedly different for reactions MR2 and MR3. Reaction MR2 has an energy barrier that is 0.60 and 0.65 eV higher than that for reaction MR1 for Zr and Hf, respectively, and is calculated to be significantly endothermic (by 1.90 and 2.13 eV). This is in strong contrast to the exothermic MR1 reactions. The difference is obviously due to the fact that the strong M−OH bond is broken in MR2 whereas the weaker $M-CH_3$ bond is broken in MR1. The methylated MR3 pathways are notable in that they have activation energies comparable to or lower than those of the MR1 reactions (1.09 and 1.19 eV) and yield surface products of stability nearly comparable to that of the surface products of the reference reactions, being 0.03 and 0.05 eV more exothermic for the Zr and Hf precursors, respectively. In this case, the reaction energetics are comparable since the same $M-CH_3$ bond is broken in both MR3 and MR1.

Overall, for both metals, when R = Cl, the reactions are less kinetically favorable than for R = CH_3. Reaction MR2 is less endothermic for the chlorides than the methyls for both metal centers. For the case of reaction MR3, it is seen that when R = Cl, the reaction is highly endothermic, but for R = CH_3, this reaction is exothermic and, hence, thermodynamically activated. Therefore, the MR3 reactions more closely resemble the basic ALD reactions than do the MR2 reactions, and furthermore, the more favored pathway for the formation of a metal-silicon linkage is predicted to be MR3.

For the hydroxylated Zr and Hf precursors, reaction MR4 results in hydroxylation of the surface reaction site and can be compared to the analogous reaction involving H_2O. As mentioned earlier, the energy barrier and overall enthalpy of reaction for H_2O reacting with the H/Si(100)-2×1 surface are 1.61 and −0.78 eV, respectively. The H_2O and MR_3OH surface hydroxylation reactions are denoted by ◇ and ◆ in Figures 1−4, respectively. In all four cases, these reactions have the lowest energy barriers of all the reactions involving the hydroxylated metal ALD precursors. The MCl_3OH and $M(CH_3)_3OH$ activation energies are found to be 0.57 and 0.64 eV and 0.56 and 0.54 eV lower in energy than the H_2O surface hydroxylation activation energy for Zr and Hf, respectively. Overall, however,

the MR4 pathways are energetically unfavorable, being endothermic by 1.38−1.55 eV. The MR2 and MR4 pathways are the only sets of deposition reactions resulting from the breaking of a strong M−O bond, and both sets are strongly endothermic, as compared to many of the competing surface reactions.

Finally, an additional reaction pathway exists for the hydroxylated ALD precursors with the H/Si(100)-2×1 surface that is unique in that it is not analogous to any of the reactions involving the MR_4 precursors or H_2O. In the MR5 surface reactions, the MCl_3OH or $M(CH_3)_3OH$ reacts with the H/Si-(100)-2×1 surface, releasing H_2 and depositing $-O-MR_3$ on the surface. This is an extremely significant chemical pathway since it results in an atomic level interface between the Si and subsequently deposited metal oxide films and is equivalent to the ALD growth species produced by an initial O-deposition half-reaction, followed by a subsequent Zr- or Hf-deposition half-reaction. The energy profile for the deposition of $-O-MR_3$ is shown in Figures 1−4 with critical point structures denoted by ●. The activation energies for the MR5 reactions range from 1.61 to 1.75 eV. However, thermodynamically it is the most favored reaction, having overall reaction enthalpies of −0.96 to −0.98 eV, significantly more exothermic than the parent precursor reactions with the H/Si(100)-2×1 surface.

IV. Conclusions

The initial surface reaction pathways of methylated and chlorinated Zr and Hf ALD precursors, the oxygen precursor H_2O, and hydroxylated metal precursors with the H/Si(100)-2×1 surface have been investigated using cluster-based density functional calculations. A comparison of the results obtained for the initial surface reactions for the methylated and chlorinated ALD metal precursors reveals key differences in relative energetics. Surface reactions involving the chlorinated precursors have sizable activation energies and are endothermic overall, whereas the methylated pathways have lower reaction barriers and are thermodynamically favorable. The H_2O ALD nucleation reaction is found to have an activation energy intermediate between those of the chlorinated and methylated metal precursors and is most exothermic. These results may have important implications for ALD nucleation on H/Si, suggesting that the tetraalkylated precursors may be better suited for initial ALD nucleation reactions than their halogen analogues, as they possess more thermodynamically favorable surface reaction pathways and exothermic products. The gas-phase hydroxylation of the metal precursors was found to be possible, being exothermic and having little or no classical barrier. The thermodynamically preferred surface reaction pathway for the hydroxylated metal precursors is the $-O-MR_3$ deposition pathway, releasing H_2.

Acknowledgment. We gratefully acknowledge computational resources provided by the University Information Technology Services (UITS), Indiana University, and NCSA (Grant No. CHE030049). M.D.H. and R.D.F. also thank the Department of Chemistry, Indiana University, for financial support provided by Ernest R. Davidson fellowships. We are grateful to G. A. Ferguson for insightful discussions.

References and Notes

(1) Muller, D. A.; Sorsch, T.; Moccio, S.; Baumann, F. H.; Evans-Lutterodt, K.; Timp, G. *Nature* **1999**, *399*, 758.

(2) Packan, P. A. *Science* **1999**, *285*, 2079.

(3) Morita, M.; Fukumoto, H.; Imura, T.; Osaka, Y.; Ichihara, M. *J. Appl. Phys.* **1985**, *58*, 2407.

(4) Kuo, C. T.; Kwor, R.; Jones, K. M. *Thin Solid Films* **1992**, *213*, 257.

(5) Wilk, G. D.; Wallace, R. M.; Anthony, J. M. *J. Appl. Phys.* **2001**, *89*, 5243.

(6) Ritala, M.; Kukli, K.; Rahtu, A.; Raisanen, P. I.; Leskela, M.; Sajavaara, T.; Keinonen, J. *Science* **2000**, *288*, 319.

(7) Suntola, T.; Hyvarinen, J. *Annu. Rev. Mater. Sci.* **1985**, *15*, 177.

(8) Copel, M.; Gribelyuk, M.; Gusev, E. *Appl. Phys. Lett.* **2000**, *76*, 436.

(9) Kukli, K.; Ritala, M.; Leskela, M.; Sajavaara, T.; Keinonen, J.; Jones, A. C.; Tobin, N. L. *Chem. Vap. Deposition* **2004**, *10*, 91.

(10) Ritala, M.; Leskela, M. *Appl. Surf. Sci.* **1994**, *75*, 333.

(11) Ritala, M.; Leskela, M.; Niinisto, L.; Prohaska, T.; Friedbacher, G.; Grasserbauer, M. *Thin Solid Films* **1994**, *250*, 72.

(12) Widjaja, Y.; Han, J. H.; Musgrave, C. B. *J. Phys. Chem. B* **2003**, *107*, 9319.

(13) Widjaja, Y.; Musgrave, C. B. *Appl. Phys. Lett.* **2002**, *81*, 304.

(14) Frank, M. M.; Chabal, Y. J.; Wilk, G. D. *Appl. Phys. Lett.* **2003**, *82*, 4758.

(15) Halls, M. D.; Raghavachari, K.; Frank, M. M.; Chabal, Y. J. *Phys. Rev. B* **2003**, *68*.

(16) Cassir, M.; Goubin, F.; Bernay, C.; Vernoux, P.; Lincot, D. *Appl. Surf. Sci.* **2002**, *193*, 120.

(17) Takahashi, N.; Yoshii, N.; Nonobe, S.; Nakamura, T.; Yoshioka, M. *J. Electron. Mater.* **2003**, *32*, 1107.

(18) Lee, J.; Koo, J.; Sim, H. S.; Jeon, H.; Won, Y. *J. Korean Phys. Soc.* **2004**, *44*, 915.

(19) Green, M. L.; Ho, M. Y.; Busch, B.; Wilk, G. D.; Sorsch, T.; Conard, T.; Brijs, B.; Vandervorst, W.; Raisanen, P. I.; Muller, D.; Bude, M.; Grazul, J. *J. Appl. Phys.* **2002**, *92*, 7168.

(20) Park, H. B.; Cho, M. J.; Park, J.; Lee, S. W.; Hwang, C. S.; Kim, J. P.; Lee, J. H.; Lee, N. I.; Kang, H. K.; Lee, J. C.; Oh, S. J. *J. Appl. Phys.* **2003**, *94*, 3641.

(21) Ganem, J. J.; Trimaille, I.; Vickridge, I. C.; Blin, D.; Martin, F. *Nucl. Instrum. Methods Phys. Res., Sect. B* **2004**, *219−20*, 856.

(22) Parmeter, J. E.; Smith, D. C.; Healy, M. D. *J. Vac. Sci. Technol., A* **1994**, *12*, 2107.

(23) Cheon, J.; Dubois, L. H.; Girolami, G. S. *J. Am. Chem. Soc.* **1997**, *119*, 6814.

(24) Wu, Y. D.; Peng, Z. H.; Chan, K. W. K.; Liu, X. Z.; Tuinman, A. A.; Xue, Z. L. *Organometallics* **1999**, *18*, 2081.

(25) Raghavachari, K.; Chabal, Y. J.; Struck, L. M. *Chem. Phys. Lett.* **1996**, *252*, 230.

(26) Konecny, R.; Doren, D. J. *J. Chem. Phys.* **1997**, *106*, 2426.

(27) Weldon, M. K.; Stefanov, B. B.; Raghavachari, K.; Chabal, Y. J. *Phys. Rev. Lett.* **1997**, *79*, 2851.

(28) Stefanov, B. B.; Gurevich, A. B.; Weldon, M. K.; Raghavachari, K.; Chabal, Y. J. *Phys. Rev. Lett.* **1998**, *81*, 3908.

(29) Halls, M. D.; Raghavachari, K. *J. Phys. Chem. A* **2004**, *108*, 2982.

(30) Frisch, M. J.; Trucks, G. W.; Schlegel, H. B.; Scuseria, G. E.; Robb, M. A.; Cheeseman, J. R.; Montgomery, J., J. A.; Vreven, T.; Kudin, K. N.; Burant, J. C.; Millam, J. M.; Iyengar, S. S.; Tomasi, J.; Barone, V.; Mennucci, B.; Cossi, M.; Scalmani, G.; Rega, N.; Peterson, G. A.; Nakatsuji, H.; Hada, M.; Ehara, M.; Toyota, K.; Fukuda, R.; Hasegawa, J.; Ishida, M.; Nakajima, T.; Honda, Y.; Kitao, O.; Nakai, H.; Klene, M.; Li, X.; Knox, J. E.; Hratchian, H. P.; Cross, J. B.; Adamo, C.; Jaramillo, J.; Gomperts, R.; Stratmann, R. E.; Yazyev, O.; Austin, A. J.; Cammi, R.; Pomelli, C.; Ochterski, J. W.; Ayala, P. Y.; Morokuma, K.; Voth, G. A.; Salvador, P.; Dannenberg, J. J.; Zakrzewski, V. G.; Dapprich, S.; Daniels, A. D.; Strain, M. C.; Farkas, O.; Malick, D. K.; Rabuck, A. D.; Raghavachari, K.; Foresman, J. B.; Ortiz, J. V.; Cui, Q.; Baboul, A. G.; Clifford, S.; Cioslowski, J.; Stefanov, B. B.; Liu, G.; Liashenko, A.; Piskorz, P.; Komaromi, I.; Martin, R. L.; Fox, D. J.; Keith, T.; A., A.-L. M.; Peng, C. Y.; Nanayakkara, A.; Challacombe, M.; Gill, P. M. W.; Johnson, B.; Chen, W.; Wong, M. W.; Gonzalez, C.; Pople, J. A. *Gaussian 03*, Revision B.02; Gaussian: Pittsburgh, PA, 2003.

(31) Becke, A. D. *J. Chem. Phys.* **1993**, *98*, 5648.

(32) Lee, C. T.; Yang, W. T.; Parr, R. G. *Phys. Rev. B* **1988**, *37*, 785.

(33) Hay, P. J.; Wadt, W. R. *J. Chem. Phys.* **1985**, *82*, 270.

(34) Hay, P. J.; Wadt, W. R. *J. Chem. Phys.* **1985**, *82*, 299.

(35) Wadt, W. R.; Hay, P. J. *J. Chem. Phys.* **1985**, *82*, 284.

(36) A single primitive Gaussian was added to each of the s, p, d, and f shells of the metal atoms. The contraction coefficients and scale factors were all set to unity. The following exponents are listed in order of increasing angular momentum (starting with s and ending with f) for the respective atom: 1.002E−02, 7.290E−03, 2.406E−02, and 2.980E−01 for Zr; 1.272E−02, 8.220E−03, 2.286E−02, and 2.930E−01 for Hf.

(37) Hariharan, P. C.; Pople, J. A. *Theor. Chim. Acta* **1973**, *28*.

(38) Widjaja, Y.; Musgrave, C. B. *J. Chem. Phys.* **2002**, *117*, 1931.

(39) Halls, M. D.; Raghavachari, K. *J. Chem. Phys.* **2003**, *118*, 10221.

(40) Halls, M. D.; Raghavachari, K. *J. Phys. Chem. B* **2004**, *108*, 4058.

(41) The M−R bond energies of the basic ALD precursors exhibit a strong dependence on the identity of R. At the B3-LYP/dzp level of theory, the M−Cl bonds energies (4.45 eV for M = Zr, 4.88 eV for M = Hf) are much greater than those for M−CH_3 (2.99 eV for M = Zr, 3.28 eV for M = Hf). Note that the difference in the bond energies of H−Cl (4.15 eV) and H−CH_3 (4.48 eV) is quite small.

(42) Akagi, K.; Tsukada, M. *Thin Solid Films* **1999**, *344*, 397.

(43) Kang, J. K.; Musgrave, C. B. *J. Appl. Phys.* **2002**, *91*, 3408.

(44) Within each combination of M and R, the B3-LYP/dzp bond strengths exhibit the following ordering: M−O > M−Cl > M−CH_3. The M−O bond energies for the molecules of the type MR_3OH are 5−6 eV. Reference 38 lists the energies of the bonds M−Cl and M−CH_3 for the molecules MR_4.